Diffusion blocking, path variability, and bifurcation of the final state in the phase separation of $Ni_3(Al,V)_{1-\delta}$ alloys

Makoto Tanimura[1] and Yasumasa Koyama[2]
[1]*Research Department, NISSAN ARC, Limited, Yokosuka, Kanagawa 237-0061, Japan*
[2]*Kagami Memorial Laboratory for Materials Science and Technology and Department of Materials Science and Engineering, Waseda University, Shinjuku, Tokyo 169-8555, Japan*

(Received 15 February 2007; revised manuscript received 10 May 2007; published 2 August 2007)

When a diffusion field has a regular atomic and/or vacancy configuration, diffusion blocking acts as a nonlinear perturbation in the diffusion kinetics and its appearance should substantially influence the temporal evolution of the macroscopic state in a diffusion-controlled phenomenon. In this study, we systematically review, on the basis of experimental results, the kinetic process of the $L1_2 \rightarrow L1_2+D0_{22}$ phase separation of $Ni_3(Al,V)_{1-\delta}$ alloys, which is dominated by long-range atomic diffusion in the diffusion field with the $L1_2$ ordered structure. Our results demonstrate that diffusion blocking actually dominates the diffusion kinetics when the size of the $L1_2$ single domains, in other words, the migration length of atoms in the $L1_2$ diffusion field, is larger than a certain critical value. Therefore, the state with the critical domain size becomes a branching point in the evolution of the macroscopic state because of the change in the diffusion kinetics. We have also found that, under the diffusion-blocking mode, the vanadium (V) content of the domain boundaries accumulated during the evolution from the initial to the branching state directly varies the kinetic path, causing a bifurcation of the final ($L1_2+D0_{22}$ or $L1_2$ single) state. These results imply that the formation of the final state should be explainable based on the kinetic description, not on the free-energy description, from the viewpoints of the blocking effect and the path variability in the kinetic process. This conversion of the description represents the discrepancy between the ensemble and time averages of the system in the present state change.

DOI: 10.1103/PhysRevB.76.054103 PACS number(s): 05.70.Ln, 82.40.Bj, 64.75.+g, 66.30.−h

I. INTRODUCTION

Temporal evolution of a state in a nonequilibrium process is generally described on the basis of a given initial condition and the subsequent kinetic path originating from that condition. When nonlinear effects dominate the nonequilibrium process, they may enhance slight differences in the initial condition over time, resulting in a complex evolution of states. As is well known in the area of nonlinear fluid system dynamics, such complex evolution of states often causes chaotic motion.

In the case of the solid state, an example of a nonequilibrium process is an irreversible relaxation from a metastable to an equilibrium state under a given thermodynamic condition. Phase separation from a metastable state is a typical example of such relaxation phenomena. The basic principle of phase separation is generally understood to be a minimization of the free energy in a closed system, which is derived from the law of increasing system entropy (i.e., the second law of thermodynamics). Thus, from a macroscopic viewpoint, the final state of the system should be at thermal equilibrium under a given thermodynamic condition, which must be "independent" of the variation in the initial conditions and/or in the kinetic paths. On the other hand, the kinetic process is microscopically controlled by long-range atomic diffusion when phase separation occurs in systems with a distribution of chemical components. As has been pointed out theoretically, a certain restriction on atomic jumps in the diffusion field has a nonlinear effect on the diffusion flow.[1,2] Our interest has been therefore focused on the temporal evolution of a macroscopic state when such nonlinearity in the microscopic diffusion kinetics exerts a significant impact on the evolution of the state.

Diffusion kinetics involving nonlinear effects is often found in alloys with substitution-type ordered structures. Because the regular atomic arrangement in an ordered structure creates preferential occupation sites for thermal vacancies, atomic jump sites are necessarily severely limited when the ordered structure serves as the diffusion field. The nonlinear effect resulting from this limitation must, to a greater or lesser degree, impact the kinetic process of the phase separation and consequent evolution of the state. From that perspective, we have systematically investigated the kinetic process of the phase separation from the metastable $L1_2(Ni_3(Al,V))$ to the equilibrium $L1_2(Ni_3Al)+D0_{22}(Ni_3V)$ phases of $Ni_3(Al,V)$ alloys.[3–7] The $L1_2$ and $D0_{22}$ structures are the A_3B-type ordered structures based on the fcc lattice and the phase separation is dominated by the long-range diffusion of B-site atoms (Al and V) in the $L1_2$ matrix.[8] It should be mentioned here that vacancies in the $L1_2$ structure show strong A site (Ni site) selectivity.[9–11]

The purpose of this paper is to describe the total picture of the temporal evolution of the macroscopic state related to the phase separation of $Ni_3(Al,V)_{1-\delta}$ alloys from the viewpoint of the microscopic diffusion kinetics. First, we will review the change in the kinetic processes of the evolution of the macroscopic state with respect to the appearance of diffusion blocking. As has been reported previously, the macroscopic state evolves to either the $L1_2+D0_{22}$ state or the metastable $L1_2$ single state depending on the degree of the nonlinear effect, i.e., the blocking effect.[3–7] Then, the crucial factor that dominates the diffusion kinetics in the $L1_2$ diffusion field

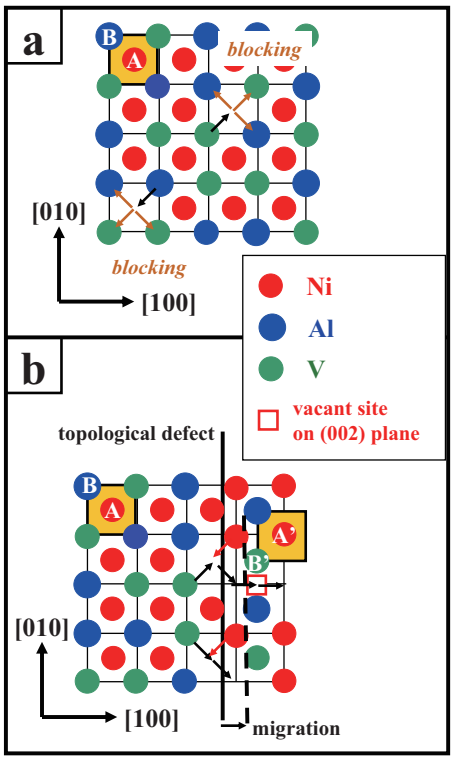

FIG. 1. (Color online) Schematic diagrams explaining the blocking effect and its relaxation. (a) Atomic arrangement on the $(001)_f$ plane in the supersaturated $L1_2$ matrix. The $A \rightarrow B$ jump of a B-site atom that has jumped to an A site is blocked due to few vacant B sites. (b) Atomic arrangement on the $(001)_f$ plane in the supersaturated $L1_2$ matrix, including a topological defect. The $B \rightarrow A \rightarrow A'$ jumps of a B-site atom as well as the $A' \rightarrow A$ jump of an A-site atom by crossing the topological defect can promote the expansion of the original $L1_2$ configuration, resulting in the migration of the topological defect. This implies that the defect migration can assist these atomic jumps and that the sequential migration enhances the atomic diffusion of the B-site atoms over a long range in the $L1_2$ matrix.

and the physical meaning of the bifurcation of the final state will be discussed.

II. DIFFUSION BLOCKING: ITS OCCURRENCE AND RELAXATION

In the case of the phase separation of $Ni_3(Al,V)_{1-\delta}$ alloys, the blocking effect in the diffusion kinetics (diffusion blocking) represents the nonlinear effect on the diffusion flow.[1,4] Let us consider the diffusion blocking that is expected to occur in the case of the $L1_2$ diffusion field. Figure 1(a) shows a schematic diagram of the $L1_2$ atomic and/or vacancy configuration on the $(001)_f$ plane, where the suffix f denotes the fcc notation. The yellow cell represents a unit of the $L1_2$ configuration in the plane, and A and B sites correspond to the face centered and edge sites in the unit, respectively. It has been reported that Al and V are randomly located on the B sites, while Ni and vacancies exist on the A sites in the $L1_2$ structure.[9–11] For simplicity, the diagram ignores antisite defects. An important feature of the $L1_2$ atomic configuration is that all of the 12 sites adjacent to one B site are A sites. Thus, the jump of a B-site atom without disturbing the $L1_2$ configuration requires at least two jumps, i.e., $B \rightarrow A \rightarrow B$ jumps. However, because thermal vacancies preferentially occupy the A sites in the $L1_2$ structure, there are fewer vacant B sites, which directly reduces the probability of the $A \rightarrow B$ atomic jump. That is, a B-site atom that has jumped to one A site hardly encounters vacant B sites other than its former one without the cooperative jumps of A-site atoms. Eventually, the small number of vacant B sites imposes a severe limitation on available jump sites of B-site atoms, producing the blocking effect in the $L1_2$ diffusion field. It should be mentioned here that the probability of an $A \rightarrow B$ jump increases when B-site vacancies are present at the supersaturated level, which would allow long-range diffusion of B-site atoms to take place. The introduction of more vacancies than the equilibrium level is ordinarily achieved by ice-water quenching from a high-temperature state.

When the topology of the atomic arrangement in the $L1_2$ structure varies, the blocking effect can be relaxed. Figure 1(b) shows the $L1_2$ atomic configuration on the $(001)_f$ plane, including a topological defect. The face-centered and edge sites in the $L1_2$ unit of the phase-changed region are denoted as A' and B', respectively. Because the presence of the topological defect destroys the selectivity of the vacant sites in the $L1_2$ atomic arrangement, a B-site atom can undergo $B \rightarrow A \rightarrow A'$ jumps by crossing the defect. It should be noted that such atomic jumps correspond to an expansion of the original $L1_2$ configuration, ideally with a cooperative $A' \rightarrow A$ jump of an A'-site atom. In other words, the occurrence of these jumps is accompanied by the migration of the topological defect [see Fig. 1(b)]. This indicates that the defect migration can assist the jumps of the B-site atoms and, there-

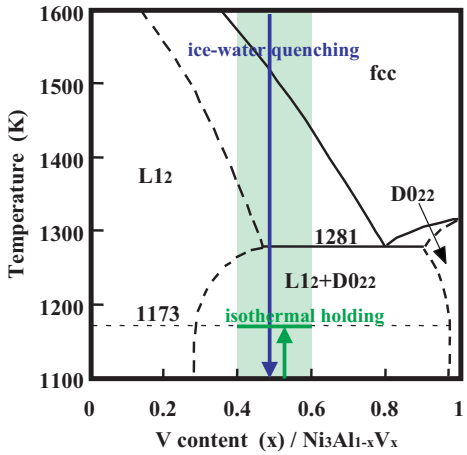

FIG. 2. (Color online) Phase diagram of pseudobinary $Ni_3Al_{1-x}V_x$ alloys.[8] The supersaturated $L1_2 \rightarrow L1_2+D0_{22}$ phase separation was induced by the following thermodynamic treatment. First, the samples cut from the $Ni_3Al_{1-x}V_x$ ingots were homogenized at 1623 K (fcc region) for 24 h, followed by quenching in ice water. It is known that the quenching treatment cannot suppress the fcc $\rightarrow L1_2$ ordering, and thus we can obtain the supersaturated $L1_2$ single state as an initial state. In order to induce the phase separation, the respective samples with the supersaturated $L1_2$ single state were kept at 1173 K ($L1_2+D0_{22}$ region) for up to 1000 h.

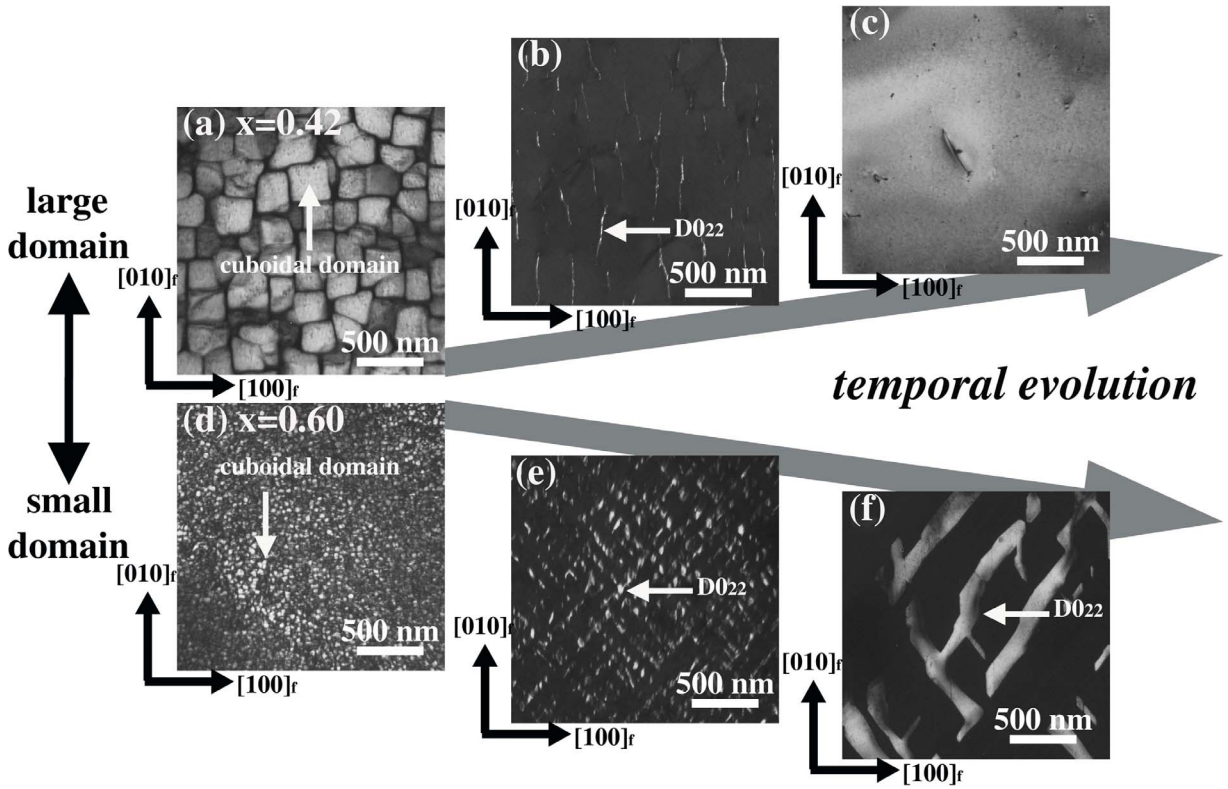

FIG. 3. Change in the microstructures of $Ni_3Al_{1-x}V_x$ alloys with $x=0.42$ and $x=0.60$ while keeping the alloys at 1173 K, observed by transmission electron microscopy. All of the images were taken under the electron incidence parallel to the $[001]_f$ direction (the suffix f denotes the fcc notation). (a) Dark-field image of the quenched $x=0.42$ alloy, taken using the 100 ordered spot due to the $L1_2$ structure. The $L1_2$ cuboidal domains with an average size of about 200 nm can be observed. (b) Dark-field image of the $x=0.42$ alloy kept at 1173 K for 1 h. The image was taken using the 1/2 10 ordered spot due to the $D0_{22}$ structure. The regions giving rise to the bright contrast and running along the $[010]_f$ direction correspond to one of three $D0_{22}$ variants (the other two variants are extended along the $[100]_f$ and $[001]_f$ directions). (c) Dark-field image of the $x=0.42$ alloy kept at 1173 K for 1000 h, taken with the 100 ordered spot. No characteristic regions except for a few lattice defects can be observed in the $L1_2$ matrix, indicating that the $x=0.42$ alloy evolves to the metastable $L1_2$ single state. (d) Dark-field image of the quenched $x=0.60$ alloy, taken using the 100 ordered spot. The size of the $L1_2$ cuboidal domains is reduced to about 30 nm on average. (e) Dark-field image of the $x=0.60$ alloy kept at 1173 K for 50 h. The image was taken using the 1/2 10 ordered spot due to the $D0_{22}$ structure. One $D0_{22}$ variant giving rise to the bright contrast is arranged along the $[110]_f$ direction. (f) Dark-field image of the $x=0.60$ alloy kept at 1173 K for 100 h, taken using the 1/2 10 ordered spot. It is clear that $D0_{22}$ growth occurred while keeping the $x=0.60$ alloy at 1173 K, resulting in the evolution to the equilibrium $L1_2+D0_{22}$ state.

fore, a continuous migration of the topological defect can enhance the diffusion of the B-site atoms over a long range by using A'-site vacancies on the $(001)_f$ or $(002)_f$ planes in the phase-changed region. This model points out the possibility that the presence of topological defects may relax diffusion blocking. It can be expected that such relaxation will be easily accomplished as the number (density) of the topological defects increases. In alloys having substitution-type ordered structures, topological defects are often introduced as antiphase boundaries.

III. CHANGE IN FINAL STATE DEPENDING ON VARIATION IN INITIAL MICROSTRUCTURE

In this section, we review the temporal evolution of the macroscopic state related to the phase separation of $Ni_3(Al,V)_{1-\delta}$ alloys on the basis of our experimental results. The features of the phase separation of this alloy system are described in the phase diagram in Fig. 2. The detailed experimental procedures and thermodynamic conditions are explained elsewhere.[3–7]

A. Evolution from initial $L1_2$ state with cuboidal domains

In stoichiometric $Ni_3(Al_{1-x}V_x)$ alloys with $0.40 \leqslant x \leqslant 0.60$, the microstructures of the supersaturated $L1_2$ matrix, obtained by ice-water quenching from the high-temperature fcc region, are characterized by the formation of cuboidal domains. It should be noted that the cuboidal domains are divided by small-angle tilt boundaries running along one of the $\langle 100\rangle_f$ directions in the $L1_2$ matrix. An important feature of the initial microstructures is that the average domain size decreases as the V content (**x**) increases. Because the details of this change are shown in Fig. 1 in Ref. 5, we briefly explain the size reduction by focusing here on the alloys with $x=0.42$ and 0.60 in Figs. 3(a) and 3(d). As shown in these micrographs, the average sizes of the cuboidal domains are about 200 nm for the $x=0.42$ alloy and 30 nm for the x

=0.60 alloy. When $0.40 \leqslant x \leqslant 0.60$ alloys are kept at a temperature in the $L1_2+D0_{22}$ region for up to 1000 h, the final state is found to bifurcate depending on the initial domain size. As shown in Figs. 3(c) and 3(f), the initial $L1_2$ microstructure with large cuboidal domains leads to the metastable $L1_2$ single state, while the $L1_2+D0_{22}$ state originates from the microstructure with small cuboidal domains. The critical size of the initial domains for this bifurcation is about 100 nm, which was obtained from quenched alloys of around $x=0.55$.[5] It should be mentioned here that the metastable $L1_2$ single state consists of large $L1_2$ grains, having an average size of more than 50 μm, with a uniform distribution of Ni, Al, and V atoms.[4] The distribution of Al and V between the $L1_2$ and $D0_{22}$ regions was confirmed for the $L1_2+D0_{22}$ state.[6]

A common characteristic in both kinetic processes is the appearance of $D0_{22}$ regions at the domain boundaries in the initial stage [see Figs. 3(b) and 3(e)]. That is, the growth or annihilation of these $D0_{22}$ regions is a key phenomenon in the bifurcation of the final state. Our detailed analysis has revealed that the suppression of $D0_{22}$ growth and consequent annihilation of $D0_{22}$ regions are caused by the occurrence of diffusion blocking.[3,4] When the $L1_2$ domains are small enough, the blocking effect does not dominate the diffusion kinetics and the $D0_{22}$ regions can grow with sequential atomic diffusion.[6] This strongly suggests that the appearance of diffusion blocking is closely related to the atomic migration distance to the domain boundaries, which is determined by the size of the $L1_2$ domains in the diffusion field.

In order to understand the dependence of the diffusion kinetics on the $L1_2$ domain size, we used analytical electron microscopy to investigate the changes in the V content of both the $D0_{22}$ precipitates and the $L1_2$ matrix as a function of the average size of the $L1_2$ cuboidal domains. Figures 4(a) and 4(b) show the changes in the average V content of the $D0_{22}$ precipitates and the $L1_2$ matrix, respectively, obtained from $x=0.45$, 0.48, 0.50, 0.55, and 0.60 alloys. We first describe the case of the $x=0.45$, 0.48, 0.50, and 0.55 alloys, which are found to evolve to the metastable $L1_2$ single state. At the initial stage, the V content of the $D0_{22}$ precipitates increases while that of the $L1_2$ matrix decreases in all the alloys, together with the growth of the $L1_2$ domains. That is, V diffusion occurs in the $L1_2$ matrix at this stage. At the latter stage, the $D0_{22}$ precipitates disappear and the V content of the $L1_2$ matrix returns to the respective initial V composition due to the occurrence of diffusion blocking. A common feature of this seemingly reversible V-content variation in the $L1_2$ matrix is that the bottom of the variation curves forms around a domain size of about 300 nm. This indicates that diffusion blocking occurs in the $L1_2$ matrix composed of cuboidal domains that are larger in size than 300 nm. As for the $x=0.60$ alloy, it is obvious that the V content of the $D0_{22}$ precipitates (the $L1_2$ matrix) increases (decreases) with the evolution to the $L1_2+D0_{22}$ state. In this case, we cannot find a clear correlation between the V-content variation and the $L1_2$ domain size. Important features of the V-content variation, however, are that the average V content of the $D0_{22}$ precipitates increases to about 0.85 before the $L1_2$ domains grow in size to about 300 nm, barely changes in the latter stage, and does not reach the equilibrium value at the final state. This indicates that diffusion blocking occurs in the latter stage even in this alloy after the domains grow in size to about 300 nm. In short, the variation in the V content in Fig. 4 clearly shows a large dependence of the diffusion kinetics on the size of the $L1_2$ single domains. The blocking effect especially dominates the diffusion kinetics in the $L1_2$ diffusion field with large cuboidal domains, where the critical domain size is about 300 nm.

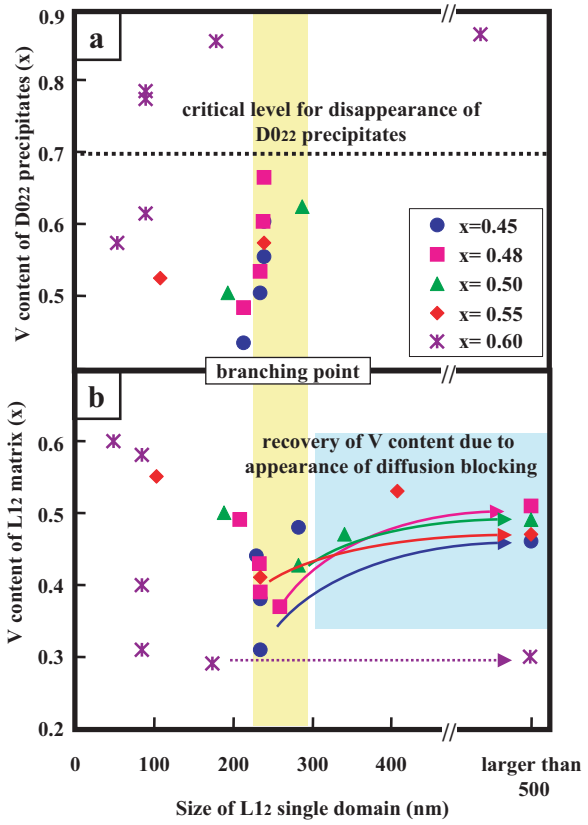

FIG. 4. (Color online) Changes in the average V content of (a) the $D0_{22}$ precipitates and (b) the $L1_2$ matrices obtained from $x=0.45$, 0.48, 0.50, 0.55, and 0.60 alloys as a function of the average size of the $L1_2$ cuboidal domains. Note that each V value was obtained by averaging several V values from the center of the $L1_2$ domains or the $D0_{22}$ precipitates.

B. Evolution from initial $L1_2$ state with antiphase domains

The initial microstructure can vary markedly when the chemical composition of $Ni_3(Al_{1-x}V_x)$ alloys deviates slightly from the stoichiometric composition. Specifically, the microstructure of the supersaturated $L1_2$ matrix of nonstoichiometric $Ni_3(Al_{1-x-y}V_x)$ alloys is characterized by the formation of antiphase domains, not cuboidal domains. Note that the antiphase domains are divided by antiphase boundaries, the introduction of which causes a topological change in the atomic and/or vacancy arrangement in the $L1_2$ matrix. The microstructures of the supersaturated $L1_2$ matrix obtained from $Ni_3(Al_{0.50-y}V_{0.50})$ alloys with $y=0.04$ and 0.08 are shown in Figs. 5(a) and 5(d) as examples. A feature of the initial microstructure is that the average size of the antiphase domains decreases with an increase in the **y** value, which is

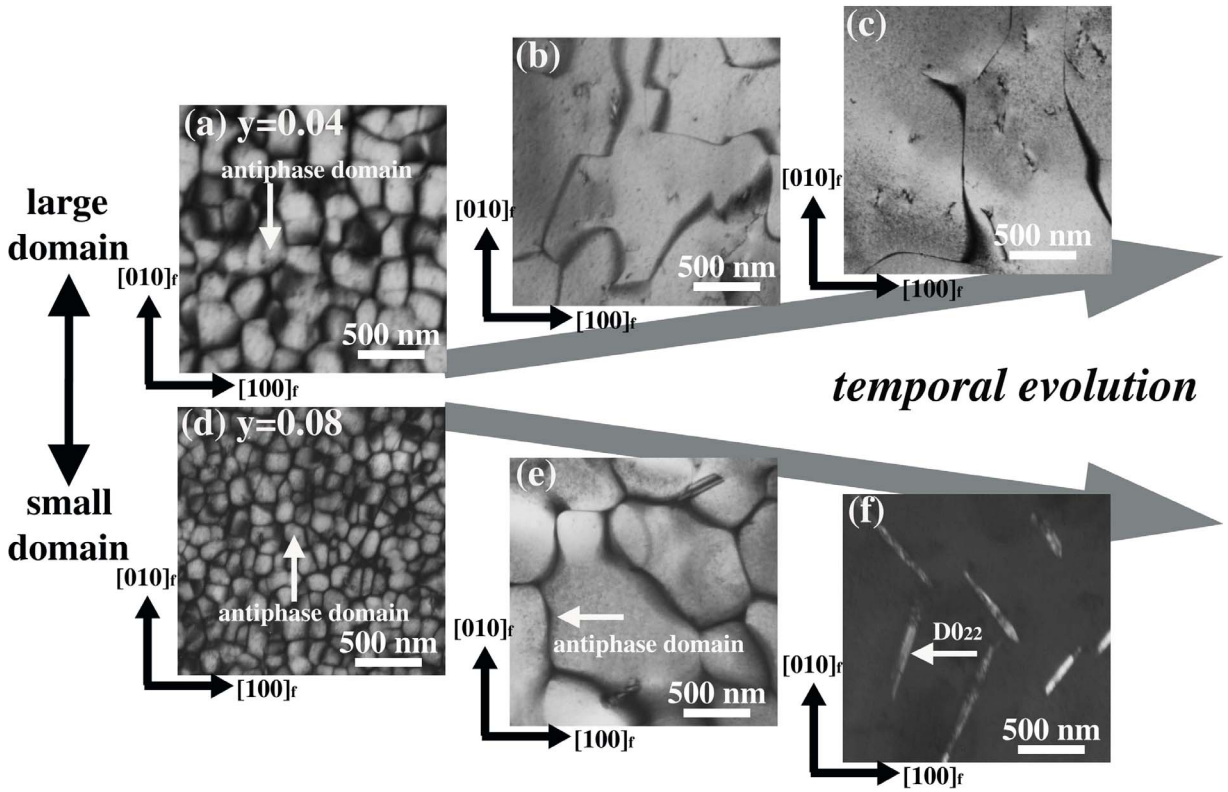

FIG. 5. Change in the microstructures of $Ni_3Al_{0.50-y}V_{0.50}$ alloys with $y=0.04$ and $y=0.08$ while keeping the alloys at 1173 K, observed by transmission electron microscopy. All of the images were taken under the electron incidence parallel to the $[001]_f$ direction. (a) Dark-field image of the quenched $y=0.04$ alloy, taken using the 100 ordered spot due to the $L1_2$ structure. Antiphase domains with an average size of about 100 nm can be observed. (b) Dark-field image of the $y=0.04$ alloy kept at 1173 K for 1 h, taken with 100 ordered spot. The size of the antiphase domains giving rise to the bright contrast increases to about 1 μm on average. (c) Dark-field image of the $y=0.04$ alloy kept at 1173 K for 100 h, taken with the 100 ordered spot. No characteristic regions except for a few lattice defects can be observed, as in the case of the $x=0.42$ alloy (d) Dark-field image of the quenched $y=0.08$ alloy, taken using the 100 ordered spot. The size of the antiphase domains is reduced to about 80 nm on average. (e) Dark-field image of the $y=0.08$ alloy kept at 1173 K for 50 h, taken using the 100 ordered spot. Antiphase domains giving rise to the bright contrast grow larger in size to about 1 μm at this stage. (f) Dark-field image of the $y=0.08$ alloy kept at 1173 K for 500 h, taken using the 1/2 10 ordered spot due to the $D0_{22}$ structure. One $D0_{22}$ variant giving rise to the bright contrast is arranged along the $[110]_f$ direction.

similar to the tendency seen for the cuboidal domains. For example, the domain size of the $y=0.04$ alloy is about 150 nm, whereas that of the $y=0.08$ alloy is 80 nm. This implies that the domain size is affected by the degree of the deviation from the stoichiometric composition of the alloys.

When quenched alloys were kept at 1173 K, the evolved state was also found to bifurcate depending on the size of the initial antiphase domains. As shown in Fig. 5(c), the final state of the $y=0.04$ alloy is the metastable $L1_2$ single state. Characteristics of the microstructure include the large $L1_2$ grains with few lattice defects and the uniform distribution of Ni, Al, and V. These features are the same as those of the metastable $L1_2$ single state evolved from large cuboidal domains. In contrast, the $y=0.08$ alloy, having an initial state composed of small antiphase domains, evolved to the $L1_2+D0_{22}$ state [see Fig. 5(f)]. Our systematic analysis revealed that the critical size of the initial antiphase domains for the bifurcation of these two final states was about 90 nm, which was obtained from quenched alloys of around $y=0.06$.

At the initial stage of both kinetic processes, the growth of the antiphase domains commonly occurs due to the migration of the antiphase boundaries [see Figs. 5(b) and 5(e)]. As was mentioned in Sec. II, the migration of the antiphase boundaries can "relax" diffusion blocking. This relaxation effect is more effective when the domain size is smaller, because the area swept by the migrating antiphase boundaries becomes larger as the antiphase boundaries increase in number. Our analysis revealed that the antiphase boundaries in Fig. 5(e) had an average V content of 0.68, larger than the value of 0.52 in Fig. 5(b), although the concentration fluctuation was quite large [see Fig. 4(a) in Ref. 7]. However, the dependence of the diffusion kinetics on the size of the $L1_2$ single domains suggests that the blocking effect should be renascent when the $L1_2$ antiphase domains grow larger in size to more than 300 nm. At that domain size, the balance between the relaxation and blocking modes becomes a crucial issue in the diffusion kinetics. The large concentration fluctuation at the antiphase boundaries is attributed to differences in this balance from place to place.

When the migration of the antiphase boundaries becomes passive, the relaxation mode is lost and diffusion blocking is dominant in the diffusion kinetics. On the basis of the size

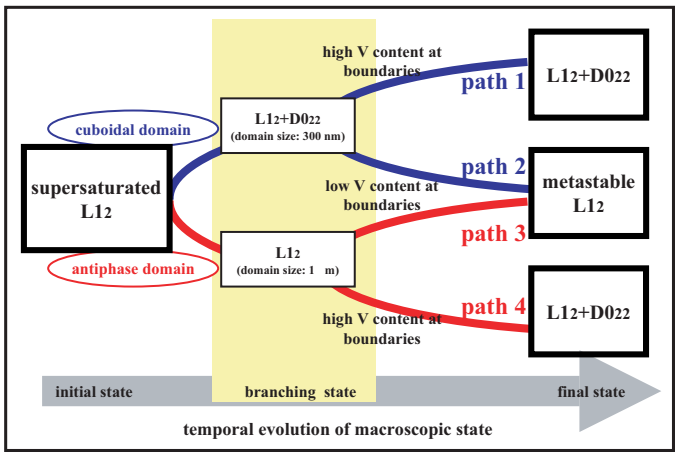

FIG. 6. (Color online) Bifurcation diagram of the kinetic processes in the phase separation of $Ni_3Al_{1-x}V_x$ alloys. The variation in the initial state, which is characterized by the formation of cuboidal or antiphase domains, first produces two types of kinetic path (denoted in blue and red). At the branching state, each process bifurcates into two processes, with the bifurcation being dominated by the average V content at the cuboidal or antiphase domain boundaries. As a result, four processes (paths 1, 2, 3, and 4) lead the state to the metastable $L1_2$ or $L1_2+D0_{22}$ state as the final state.

dependence of the diffusion kinetics, an imbalance should appear together with an increase in the size of the antiphase domains. Our research has revealed that the average V content of the $D0_{22}$ regions did not reach the equilibrium level even after the $y=0.08$ alloy was kept at 1173 K for more than 1000 h.[7] This is experimental evidence that diffusion blocking actually controls the diffusion kinetics at the latter stage. Our rough estimation suggests that a critical domain size for the appearance of the imbalance kinetics is about 1 μm (the branching state), which corresponds to the size shown in Fig. 5(b) and 5(e). It is concluded that a crucial factor for the bifurcation of the final states is the V content of the antiphase boundaries at the branching state, which is similar to the case of the stoichiometric $Ni_3(Al_{1-x}V_x)$ alloys composed of cuboidal domains.

IV. VARIABILITY OF KINETIC PATHS DURING TEMPORAL EVOLUTION OF STATES

The experimental results have revealed that two types of initial $L1_2$ microstructures lead to certain kinetic paths owing to the variation in the microscopic diffusion kinetics. We schematically summarize these paths in Fig. 6 and discuss the dependence of the paths on the features of the initial microstructures.

When the initial state is characterized by the formation of cuboidal domains, the upper (blue) case in Fig. 6, the selectivity of the vacant sites is basically maintained in the $L1_2$ diffusion field. In the process from the initial to the branching state, the $D0_{22}$ regions precipitate at the domain boundaries, accompanied by long-range V diffusion. The occurrence of V diffusion is attributed to the short migration distance of V to the domain boundaries in the $L1_2$ cuboidal domains as well as to the B-site vacancies at the supersaturated level. In the latter process, diffusion blocking dominates the diffusion kinetics and the kinetic path is classified into two types. Note that the branching state is characterized by the size of the $L1_2$ cuboidal domains, about 300 nm on average. If the V content of the $D0_{22}$ precipitates is not sufficient (less than about 0.70), the $D0_{22}$ precipitates disappear due to the blocking effect and the macroscopic state returns to the $L1_2$ single state. The kinetic path characterized by this process is denoted as path 2. On the other hand, the $D0_{22}$ precipitates remain to the end of the process when their V content at the branching state is more than 0.70 (path 1).

For the initial state with many antiphase domains, the lower (red) case in Fig. 6, the selectivity of the vacant sites in the $L1_2$ matrix is broken due to the topological change in the atomic and/or vacancy arrangement. The initial step of the evolution is the growth of the antiphase domains together with the migration of the antiphase boundaries, which can be accompanied by long-range V diffusion. Because diffusion blocking appears with the growth of the antiphase domains, the diffusion kinetics is under a mixed mode, i.e., a combination of relaxation and blocking modes together with the increase in the domain size. In the process from the branching to the final state, diffusion blocking is dominant in the diffusion kinetics. Note that the V content of the antiphase boundaries at the branching state determines the kinetic path in this process. Concretely, the state evolves to the metastable $L1_2$ state when the V content of the antiphase boundaries is small (path 3), while the $D0_{22}$ regions appear at the high V-content boundaries (path 4).

As shown in the bifurcation diagram in Fig. 6, a common and crucial future in the case of both stoichiometric and nonstoichiometric alloys is the existence of the branching state, although the domain size characterizing the state differs between the cuboidal and antiphase domains. Another common phenomenon seen in the initial process from the initial to the branching state is that the V atoms in the domains migrate to respective domain boundaries. In the process from the branching to the final state, the average V content of the domain boundaries at the branching state determines the subsequent kinetic path. Because the temporal evolution is described as one stochastic process, i.e., the accumulation of each change in the state from one instant to the next, beginning with the initial state, the features of the branching state obviously originate from those of the initial state. On this basis, it is concluded that the microstructure features of the initial state directly determine the variability of the kinetic paths and the bifurcation of the final state during the temporal evolution of the macroscopic state in accordance with the features of the branching state.

V. DISCUSSION

The foregoing review of the experimental results revealed that in the phase separation of $Ni_3(Al,V)_{1-\delta}$ alloys the appearance of diffusion blocking in the $L1_2$ diffusion field substantially restricts the formation of the equilibrium $L1_2+D0_{22}$ state of the alloys during the kinetic process. A notable consequence of the restriction is that the evolution to

the metastable $L1_2$ state occurs in a very slow kinetic process. In many cases, metastable states such as the amorphous and glass states are obtained in a rapid process. For instance, it is well known that the amorphous state is basically formed by rapid quenching from the liquid (or high-temperature solid solution) state. In contradistinction to this, we obtained the metastable $L1_2$ state by keeping the alloys at a certain temperature for a long duration, e.g., for 1000 h. Because of this slow process, the evolution to the metastable $L1_2$ state is essentially caused by the complicated diffusion kinetics in the $L1_2$ diffusion field.

A first and important question that one might pose here is whether the evolved $L1_2$ state is actually the final state or not. Two notable features of the evolved $L1_2$ state compared with the initial $L1_2$ state are the smaller fluctuation of the chemical components (Ni, Al, and V) and the presence of fewer lattice defects.[4] It is evident that the driving force for $D0_{22}$ precipitation in the evolved $L1_2$ state is reduced in comparison with that in the initial $L1_2$ state from the viewpoint of the gradient of the chemical potential. Therefore, within the traditional free-energy description, there are no physical reasons for the occurrence of $D0_{22}$ precipitation in the evolved $L1_2$ state as long as the initial $L1_2$ state does not undergo $L1_2+D0_{22}$ evolution. Although the final state cannot be confirmed experimentally (the time needed for confirmation is far beyond what is possible in the laboratory), we consider that the evolved $L1_2$ state is the final state in the present kinetics.[12]

The formation of the $L1_2$ state as the final state is strongly "dependent" on the kinetic process, which is quite different from the traditional understanding of the evolution of states related to the phase separation in the solid state under the slow kinetics. As mentioned earlier, the diffusion kinetics in the $L1_2$ matrix largely depends on the size of the $L1_2$ single (cuboidal or antiphase) domains. This indicates that the coherency of the atomic arrangement in the $L1_2$ diffusion field substantially impacts the diffusion kinetics. Considering the critical domain size (300 nm) for the appearance of diffusion blocking, the critical migration length for the restriction of long-range atomic diffusion can be estimated to be less than 100 nm. In other words, the probability for V atoms to migrate via 100-nm jumps in the $L1_2$ diffusion field is inherently zero due to diffusion blocking. Therefore, the local distribution of V at each stage in the kinetic process is important for the subsequent annihilation or remanence (formation) of the $D0_{22}$ precipitates. Because the diffusion kinetics varies together with the development of the coherent length, the temporal evolution of the state is dependent on when the coherent length reaches the critical value. It is obvious that the initial $L1_2$ state composed of smaller domains has an advantage for V aggregation ($D0_{22}$ precipitation) over a state composed of larger domains with respect to the smaller coherent length and the longer growth time to the critical size. Actually, differences in the initial state cause a variation in the branching state with respect to the distribution of chemical components and this variation determines the path variability in the latter process, resulting in the bifurcation of the final state. This "accidental" kinetic path and consequent final-state bifurcation cannot be derived from the ordinal free-energy description. It is therefore concluded that the dependence of the diffusion kinetics on the coherency of the diffusion field requires a conversion of the free-energy description to the kinetics description in order to understand the formation of the metastable $L1_2$ state as the final state.

In terms of the physics involved, this conversion signifies the nonequivalence between ensemble averaging and time averaging during the kinetic process. In general, an energy-minimum equilibrium state of a system is defined on the basis of the ensemble average of feasible microscopic states (from the viewpoint of entropy, the maximization of the number of feasible microscopic states is desired). In the case of the present phase separation, the formation of the $L1_2+D0_{22}$ state originates from the requirement for the ensemble average under the given thermodynamic parameters. The change in a macroscopic state is generally described based on time averaging, which is defined as the assembly of the feasible states created by the evolution of each single state with time.[1] The inconsistency between the evolved state and the thermal equilibrium state under the very slow kinetics represents the nonequivalence, because the averaging over an extended time period does not correspond to the ensemble averaging. It should be noted that the state evolves not along a simple energy-minimizing trajectory but along a probabilistic trajectory due to the diffusion kinetics with the strong nonlinear perturbation, i.e., the blocking effect. Thus, the nonequivalence can become conspicuous in the present case, as has been reported in the case of soft matters by Tanaka *et al.*[13]

In conclusion, we demonstrate an example in the solid state that slight differences in the initial condition can be enhanced over time due to nonlinear effects, resulting in a complex evolution of the state. The dependence of the diffusion kinetics on the coherency of the $L1_2$ diffusion field suggests that the final state can bifurcate under the same isothermal-keeping process even in a $Ni_3(Al,V)$ alloy with an identical composition, when the initial domain size of the $L1_2$ matrix varies. In other words, our results suggest the potentiality of chaotic motion appearing in the evolution of the macroscopic state in alloys in cases where the nonequivalence between ensemble averaging and time averaging is valid.

VI. CONCLUSION

It has been pointed out theoretically that, in a nonequilibrium process with long-range atomic diffusion, diffusion blocking acts as a nonlinear perturbation in the diffusion kinetics. Very recently, we have found that diffusion blocking appears in the kinetic process of the $L1_2 \rightarrow L1_2+D0_{22}$ phase separation of $Ni_3(Al_{1-x}V_x)$ alloys. In this study, we have demonstrated that the phase separation should be described on the basis of the kinetic description from the viewpoints of the blocking effect, the variability of the kinetic path, and the bifurcation of the final state. Concretely, the migration length of atoms in the $L1_2$ diffusion field is a crucial factor in the appearance of diffusion blocking and the timing of the change in the diffusion kinetics directly influences the formation of the final state. This temporal evolution of the mac-

roscopic state cannot be described by the ordinal free-energy description. In conclusion, we strongly believe that our results demonstrate a discrepancy between the ensemble and time averages of the system. In this case, the state can evolve in a complex fashion depending on slight differences in the initial condition, which indicates a possibility for the occurrence of chaotic motion even in the solid state.

ACKNOWLEDGMENTS

The authors acknowledge the technical support of T. Doi at Waseda University. This study was partially supported by a Ministry of Education, Science, Sports and Culture Grant-in-Aid for Scientific Research (B), Grant No. 18360306, 2006.

[1] H. Sato and R. Kikuchi, Phys. Rev. B **28**, 648 (1983).
[2] H. Sato, T. Ishikawa, and R. Kikuchi, J. Phys. Chem. Solids **46**, 1361 (1985).
[3] M. Tanimura, M. Kikuchi, and Y. Koyama, J. Phys.: Condens. Matter **14**, 7053 (2002).
[4] M. Tanimura, A. Hirata, and Y. Koyama, Phys. Rev. B **70**, 094111 (2004).
[5] M. Tanimura and Y. Koyama, J. Phys.: Condens. Matter **17**, 4911 (2005).
[6] M. Tanimura, T. Doi, and Y. Koyama, Mater. Trans. **46**, 2988 (2005).
[7] M. Tanimura and Y. Koyama, Acta Mater. **54**, 4385 (2006).
[8] Y. Hong, Y. Mishima, and T. Suzuki, Mater. Res. Soc. Symp. Proc. **133**, 429 (1989).
[9] H. Numakura, T. Ikeda, M. Koiwa, and A. Almazouzi, Philos. Mag. A **77**, 887 (1998).
[10] K. Badura-Gergen and H.-E. Schaefer, Phys. Rev. B **56**, 3032 (1997).
[11] M. de Koning, C. R. Miranda, and A. Antonelli, Phys. Rev. B **66**, 104110 (2002).
[12] One sure thing is that the formation of the equilibrium $L1_2 + D0_{22}$ state in the distant future must be caused by a large oscillation of the chemical-composition distribution beyond the fluctuation level, due to the reappearance (appearance $\rightarrow$ annihilation $\rightarrow$ appearance) of the $D0_{22}$ precipitates. If it occurs, this composition oscillation poses another important issue for the nonequilibrium process in the solid state.
[13] H. Tanaka, Y. Nishikawa, and T. Koyama, J. Phys.: Condens. Matter **17**, L143 (2005).